Mem-fractive Properties of Mushrooms

Alexander E. Beasley[1,2], Mohammed-Salah Abdelouahab[3], René Lozi[4], Michail-Antisthenis Tsompanas[1], Anna L. Powell[1], Andrew Adamatzky[1]

[1] Unconventional Computing Laboratory, UWE, Bristol, UK
[2] Centre for Engineering Research, University of Hertfordshire, UK
[3] Laboratory of Mathematics and their interactions, University Centre Abdelhafid Boussouf, Mila 43000, Algeria
[4] Université Côte d'Azur, CNRS, LJAD, Nice, France

E-mail: alex.e.beasley@bath.edu

Abstract. Memristors close the loop for I-V characteristics of the traditional, passive, semi-conductor devices. A memristor is a physical realisation of the material implication and thus is a universal logical element. Memristors are getting particular interest in the field of bioelectronics. Electrical properties of living substrates are not binary and there is nearly a continuous transitions from being non-memristive to mem-fractive (exhibiting a combination of passive memory) to ideally memristive. In laboratory experiments we show that living oyster mushrooms Pleurotus ostreatus exhibit mem-fractive properties. We offer a piece-wise polynomial approximation of the I-V behaviour of the oyster mushrooms. We also report spiking activity, oscillations in conduced current of the oyster mushrooms.

Keywords: Memory architecture, biological systems, memristors

Submitted to: *Bioinspir. Biomim.*

1. Introduction

Originally proposed by Chua in 1971 [1], the memristor poses a fourth basic circuit element, whose characteristics differ from that of R, L and C elements. Going through a more general point of view, Chua with coauthors Abdelouahab and Lozi [2], using fractional calculus, published 43 years after his original intuition, a global theory of family of electric elements: the memfractance theory which is the most general theory of such elements with memory, enlarging this family to mem-capacitive and mem-inductive elements of first, second third, etc. order.

In the memfractance theory the pinch observed in the voltage-current curves of the memristor is only a particular case (Figs. 1 and 2) of this memfractive electric element, allowing more flexibility in modeling.

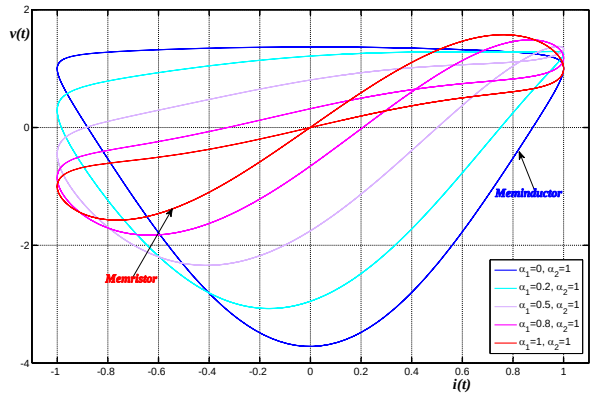

Figure 1. Ideal plot of voltage-current memfractive elements: from memristor to meminductor. [2].

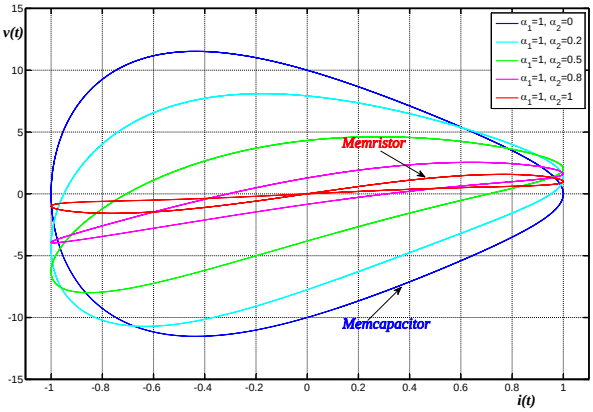

Figure 2. Ideal plot of voltage-current memfractive elements: from memristor to memcapacitor [2].

Memristance has been seen in nano-scale devices where electronic and ionic transport are coupled under an external bias voltage. Strukov *et al.* [3] posit that the hysteric I-V characteristics observed in thin-film, two-terminal devices can be understood as memristive. However, this is observed behaviour of devices that already have other, large signal behaviours.

The ideal memristor model (Figs. 1, 2) is shown to display 'lobes' on the I-V characterisation sweeps, indicating that the current resistance is a function of the previous resistance — hence a memristor has memory. For the purposes of analysis, graphs are referred to by their quadrants, starting with quadrant one as the top right and being numbered anti-clockwise.

Similarly, the mem-capacitor and mem-inductor exhibit a change in capacitance/inductance as a function of the applied voltage being swept. The introduction of the mem-capacitor and mem-inductor in [2, 4] complete the non-binary solution space of the mem-fractor that exerts a device may exhibit a combination of memristive, mem-inductor and mem-capacitor elements.

Finding a true memristor is by no means an easy task. Nevertheless, a number of studies have turned to nature to provide the answer, with varying success. Memristive properties of organic polymers were discovered before the 'official' discovery of the memristor was announced in [3]. The first examples of memristors could go back to the singing arc, invented by Duddell in 1900, which was originally used in wireless telegraphy before the invention of the triode [5]. In addition, memristive properties of organic polymers have been studied since 2005 in experiments focussing on hybrid electronic devices based on the polyaniline-polyethylenoxide junction [6]. Memristive properties of living creatures, their organs and fluids have been demonstrated in skin [7, 8, 9], blood [10], plants [11, 12] (including fruits [13, 14]), slime mould [15, 16], tubulin microtubules [17, 18, 19]. Most recent results include DNA and melanin based memristive devices [20], biomaterials extracted from plant tissue [21].

This paper presents a study of the I-V characteristics of the fruit bodies of the grey Oyster fungi *Pleurotus ostreatus*. Why fungi? Previously we recorded extracellular electrical potential of Oyster's fruit bodies, basidiocarps [22] and found that the fungi generate action potential like impulses of electrical potential. The impulses can propagate as isolated events, or in trains of similar impulses. Further, we demonstrated, albeit in numerical modelling, that fungi can be used as computing devices, where information is represented by spikes of electrical activity, a computation is implemented in a mycelium network and an interface is realised via fruit bodies [23]. A computation with fungi might not be useful *per se*, because the speed of spike propagation is substantially lower than the clock speed in conventional computers. However, the fungal computation becomes practically feasible when embedded in a slow developing spatial process, e.g. growing architecture structures. Thus, in [24] we discussed how to: produce adaptive building constructions by developing structural substrate using live fungal mycelium, functionalising the substrate with nanoparticles and polymers to make mycelium-based electronics, implementing sensorial fusion and decision making in the fungal electronics.

Why we are looking for mem-fractive properties of fungi? Mem-fractors [2] have combinations of properties exhibited by memristors, mem-capacitors and mem-inductors. A memristor is a material implication [25, 26] and can, therefore, can be used for constructing other logical circuits, statefull logic operations [25], logic operations in passive crossbar arrays of memristors [27], memory aided logic circuits [28], self-programmable logic circuits [29], and memory devices [30]. If strands of fungal mycelium in a mycelium bound composites and the fruit bodies show some mem-fractive properties then we can implement a variety of memory and computing devices embedded directly into architectural building materials made from the fungal substrates [24] and living fungal wearables [31, 32]. The field of living fungal wearables is currently in its infant stage, however it showed undeniably slim shape, good adaptability, and very low energy consumption compared to artificial wearable sensory devices [33]. Mycelium bound composites — masses of organic substrates colonised by fungi — are future environmentally sustainable growing biomaterials [34, 35, 36], already they are used in

acoustic [37, 38, 39] and thermal [40, 41, 42, 43, 44, 45] insulation wall cladding and packaging materials [46, 47, 48].

In [24] it is proposed to develop a structural substrate by using live fungal mycelium, functionalise the substrate with nanoparticles and polymers to make mycelium-based electronics, implement sensorial fusion and decision making in the mycelium networks [64] and to grow monolithic buildings from the functionalised fungal substrate [65]. Fungal buildings would self-grow, build, and repair themselves subject to substrate supplied, use natural adaptation to the environment, sense all that humans can sense. To implement sensorial integration and make decisions fungal materials will require electronic circuits, the fungal memristors will form essential part of the circuits.

The approach taken in the paper has a two-fold novelty component. First, we focus on memfractive properties of a substrate, which offers more fuzzy logic like approach of the IV properties of materials. Second, we study electrical IV properties of fungi, which are per se is a novel substrate for future organic electronics.

The rest of this paper is organised as follows. Section 2 details the experimental set up used to examine the I-V characteristics of fruit bodies. Section 3 presents the results from the experimentation. Mathematical modelling of the mem-fractive behaviour of the Grey Oyster mushrooms is given in Section 4. A discussion of the results is given in Section 5 and finally conclusions are given in Section 3.

2. Experimental Set Up

We used grey Oyster fungi *Pleurotus ostreatus* (Ann Miller's Speciality Mushrooms Ltd, UK) cultivated on wood shavings. The iridium-coated stainless steel sub-dermal needles with twisted cables (Spes Medica SRL, Italy) were inserted in fruit bodies (Fig. 3) of grey Oyster fungi using two different arrangements: 10 mm apart in the cap of the fungi (cap-to-cap), Fig. 3(a), and translocation zones (cap-to-stem), Fig. 3(b). I-V sweeps were performed on the fungi samples with Keithley Source Measure Unit (SMU) 2450 (Keithley Instruments, USA) under the following conditions: [-500 mV to 500 mV, -1 V to 1 V] with the samples in ambient lab light (965 Lux). Varying the step size of the voltage sweep allowed testing the I-V characteristics of the subject at different frequencies. The voltage ranges are limited so as not to cause the electrolysis of water. Each condition was repeated at least six times over the samples. Voltage sweeps were performed in both directions (cyclic voltammetry) and plots of the I-V characteristics were produced.

MATLAB was used to analyse the frequency and distribution of spiking behaviour observed in the I-V sweeps of the fruiting bodies under test (Sect. **??**). All histogram plots are binned according to the voltage interval set for the Kiethley SMU.

(a)

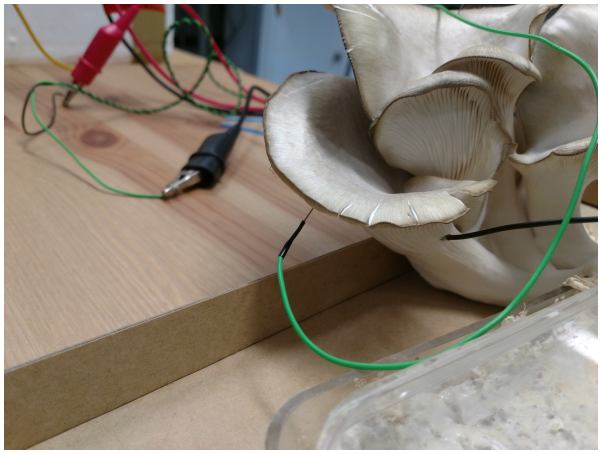

(b)

Figure 3. Positions of electrodes in fruit bodies. (a) Electrodes inserted 10 mm apart in the fruit body cap. (b) One electrode is inserted in the cap with the other in the stem.

3. Results

Fruit body samples are shown to exhibit memristive properties when subject to a voltage sweep. The ideal memristor model has a crossing point at 0V, where theoretically no current flows. Figures 4 and 5 show the results of cyclic voltammetry of Grey Oyster fungi with electrodes positioned both in the fungi caps and stems. From Figs. 4 and 5, it can be seen that when 0 V is applied by the source meter, a reading of a nominally small voltage and current is performed. The living membrane is capable of generating potential across the electrodes, and hence a small current is observed. Mem-capacitors produce similar curves to that of an ideal memristor in Fig. 1, when plotting charge (q) against voltage (v) [49]. Additionally, mem-inductors produce similar plots for current

(i) against flux (φ). However, the crossing point in the curves observed in quadrant 3 results to a pinched hysteresis loop. That is an indication that the cyclic voltammetry measurement is provided by a device that has mem-fractance properties.

While the sample under test is subjected to a positive voltage (quadrant 1), it can be seen there is nominally a positive current flow. Higher voltages result in a larger current flow. For an increasing voltage sweep there is a larger current flow for the corresponding voltage during a negative sweep.

Similarly, in quadrant 3 where there is a negative potential across the electrodes, the increasing voltage sweep yields a current with smaller magnitude than the magnitude of the current on a negative voltage sweep. Put simply, the fruit body has a resistance that is a function of the previous voltage conditions.

By applying averaging to the performed tests, a clear picture is produced that demonstrates for a given set of conditions, a typical response shape can be expected (Figs. 6 and 7). The stem-to-cap placement of the electrodes in the fruit body yields a tighter range for the response (Figs. 6(b) and 7(b)). This can be expected due to the arrangement of the transportation pathways, so-called translocation zone distinct from any vascular hyphae [50, 51], in the fruit body which run from the edge of the cap and down back through the stem to the root structure (mycelium). Cap-to-cap placement of the electrodes applies the potential across a number of the solutes translocation pathways and hence yields a wider range of results. However, for all results, it is observed that the positive phase of the cyclic voltammetry produces a different conduced current than the negative phase. The opening of the hysteresis curve around point zero suggests the fungus is not an ideal mem-ristor, instead it is also exhibiting mem-capacitor and mem-inductor effects. The build of charge in the device prevents the curve from closing completely to produce the classic mem-ristor pinching shape.

Reducing the voltage step size (by ten fold, i.e. to 0.001 V) for the I-V characterisation is synonymous to reducing the frequency of the voltage sweep. Decreasing the sweep frequency of the voltage causes the chances of "pinching" in the I-V sweep to increase, as seen in quadrant 1 of Fig. 8. This further reinforces the presence of some mem-capacitor behaviour. Since the charging frequency of the fungus has now been reduced there is a greater amount of time for capacitively stored energy to dissipate, thus producing a more 'resistive' plot with a pinch in the hysteresis. However, as indicated by two subsequent runs of voltammetry (Fig. 8), the electrical behaviour of the fungus is heavily altered under these frequencies and, thus, the repeatable observation of similar curves can not be realised (as it was observed in the aforementioned measurements and especially the stem to cap electrode placement). Nonetheless, the production of the curves can be controlled more efficiently by selecting appropriate frequencies of operation, but less successfully from the fungus substrate part, as this is a living substrate that has inherent stohasticity in the way it metabolises and grows.

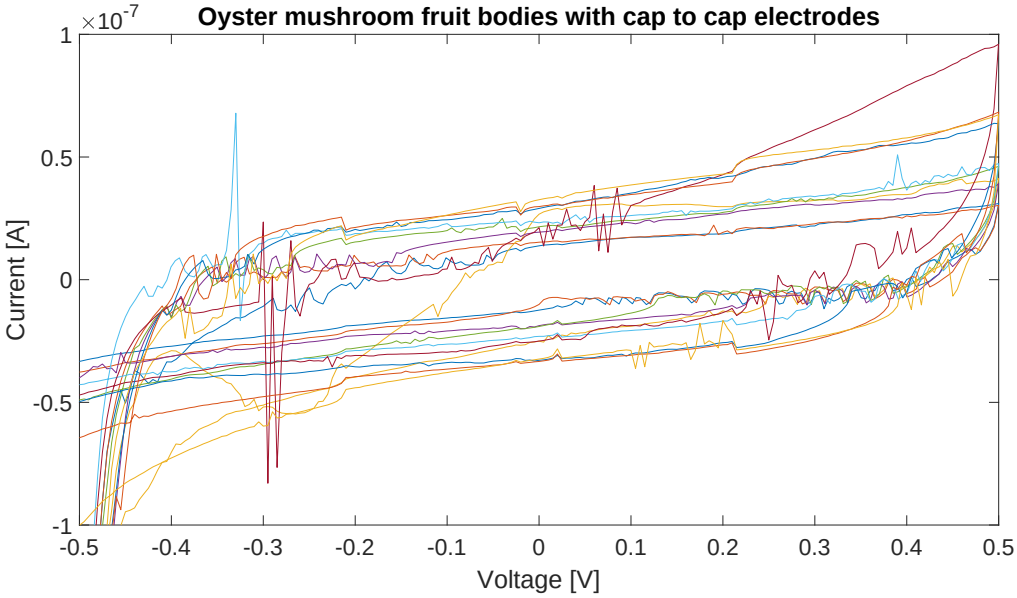

(a)

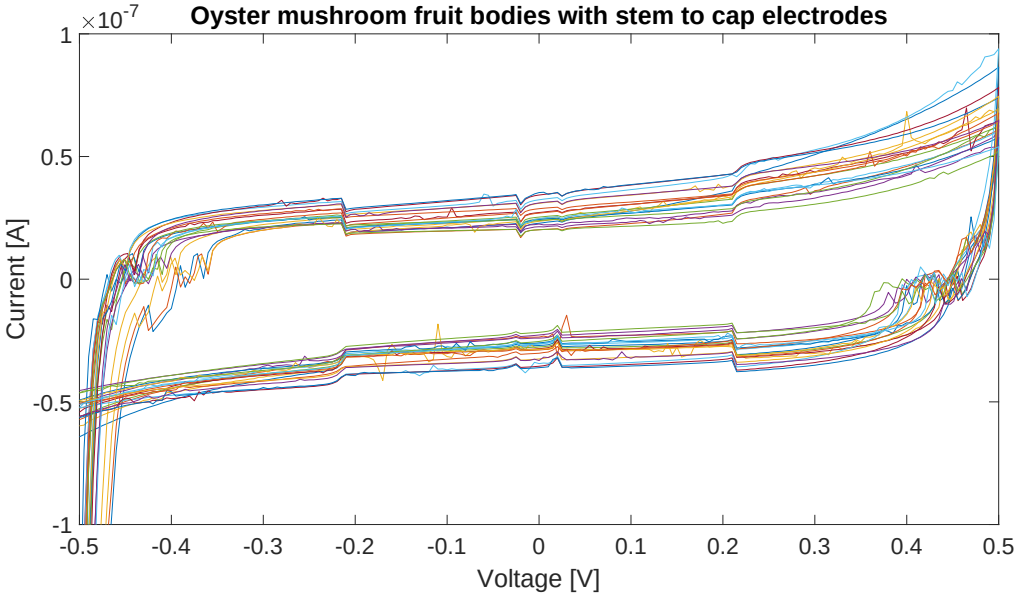

(b)

Figure 4. Raw data from cyclic voltammetry performed over -0.5 V to 0.5 V. (a) Cap-to-cap electrode placement. (b) Stem-to-cap electrode placement.

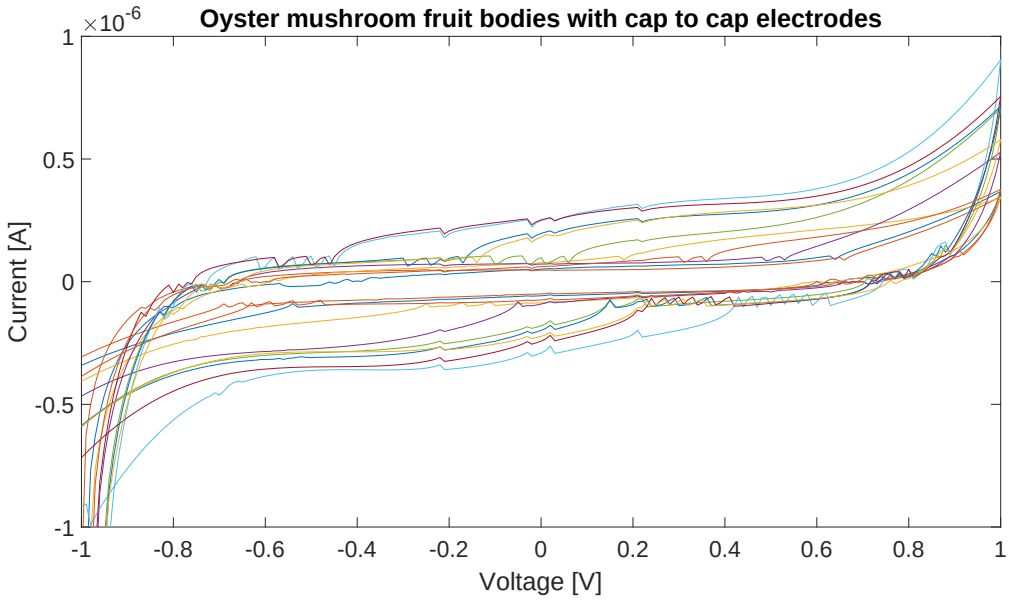

(a)

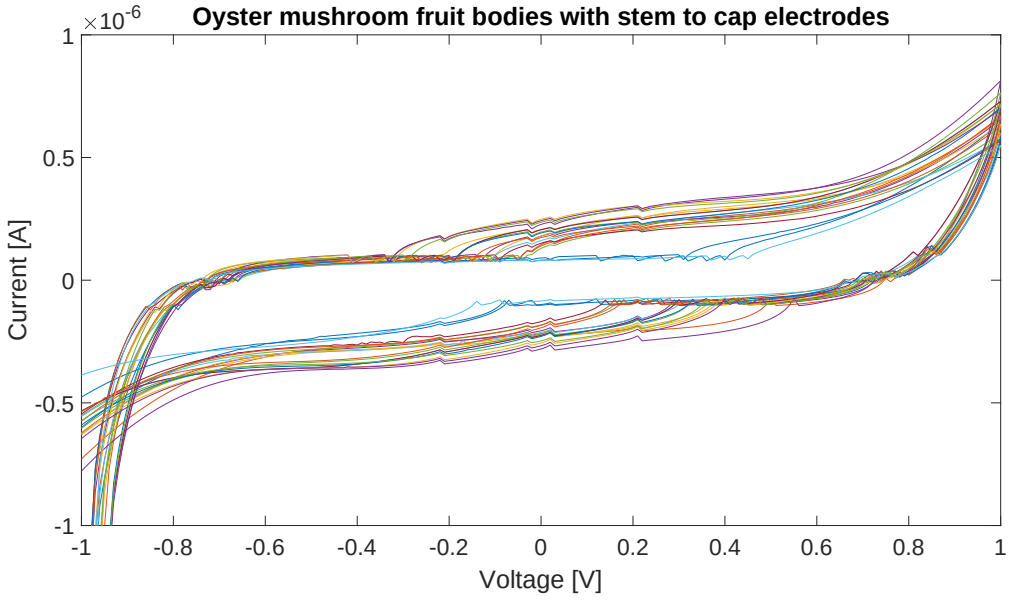

(b)

Figure 5. Raw data from cyclic voltammetry performed over -1 V to 1 V. (a) Cap-to-cap electrode placement. (b) Stem-to-cap electrode placement.

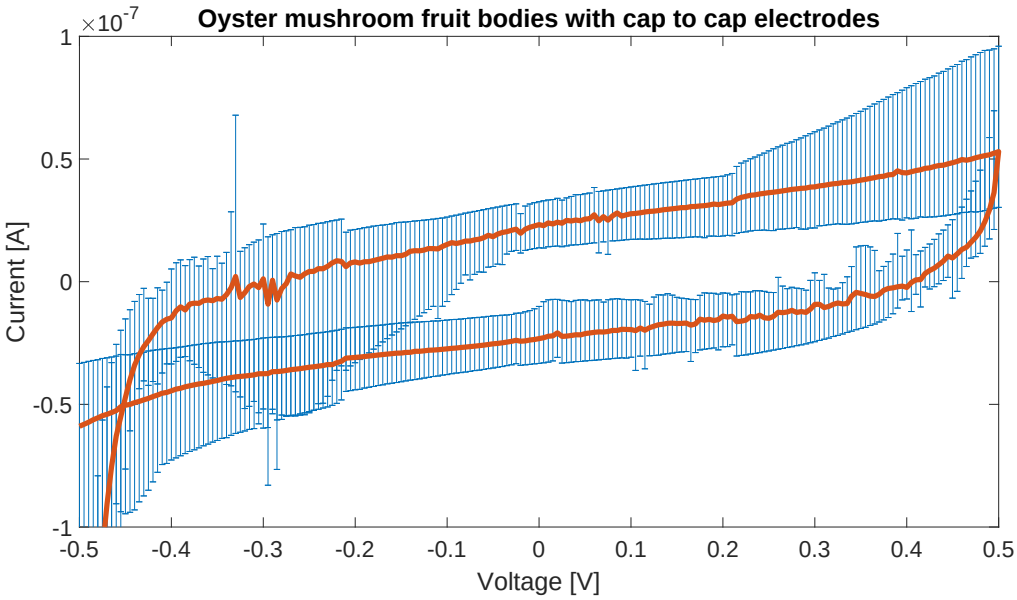

(a)

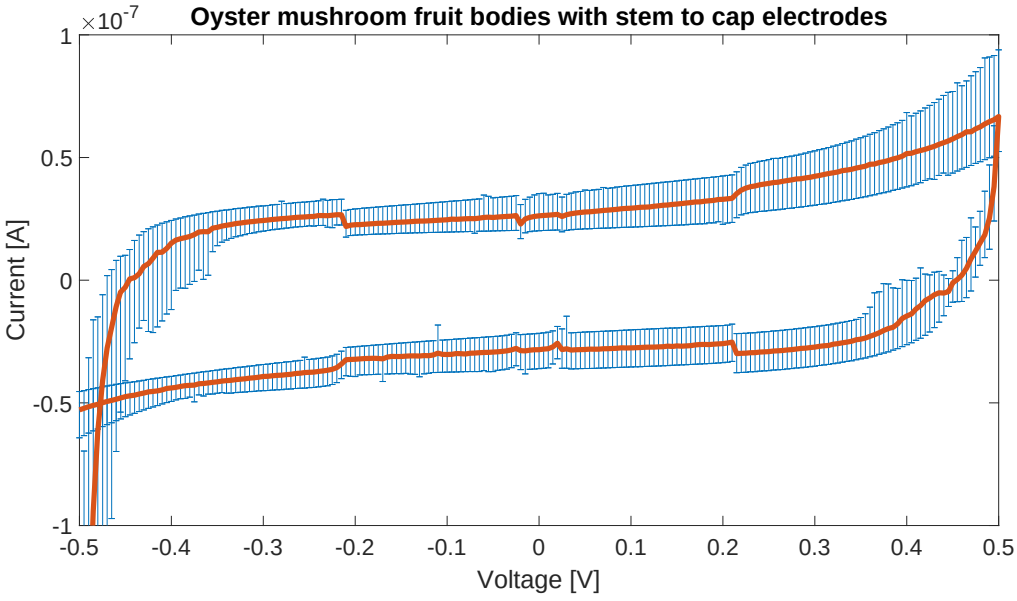

(b)

Figure 6. Average grey Oyster fungi fruit bodies I-V characteristics for cyclic voltammetry of -0.5 V to 0.5 V. (a) Cap-to-cap electrode placement. (b) Stem-to-cap electrode placement.

4. Mathematical Model of Mushroom Mem-fractance

Here we report the I-V characteristics of grey Oyster fungi *Pleurotus ostreatus* fruit bodies. It is evident from the results that grey Oyster fungi display memristive

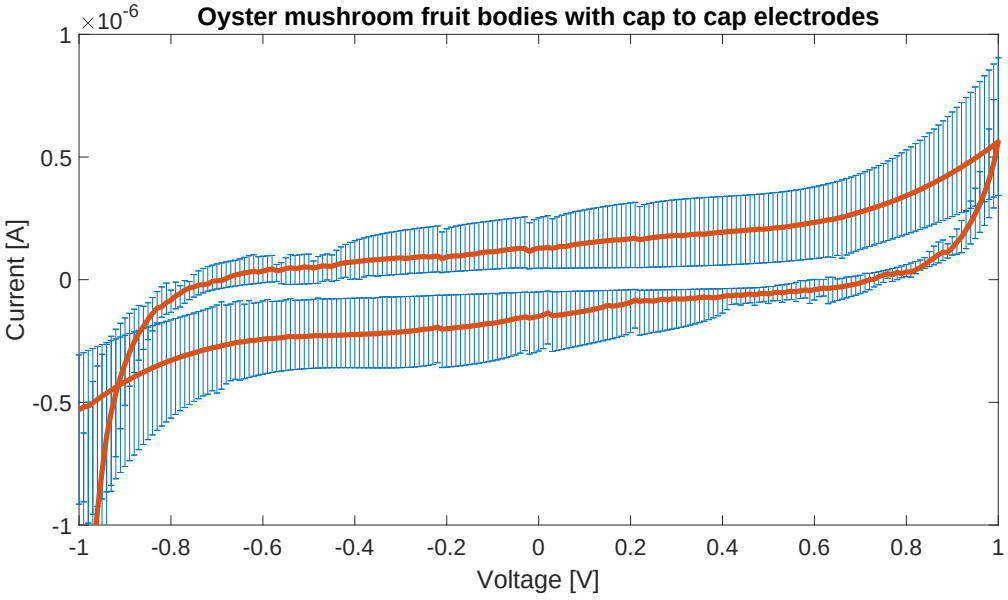

(a)

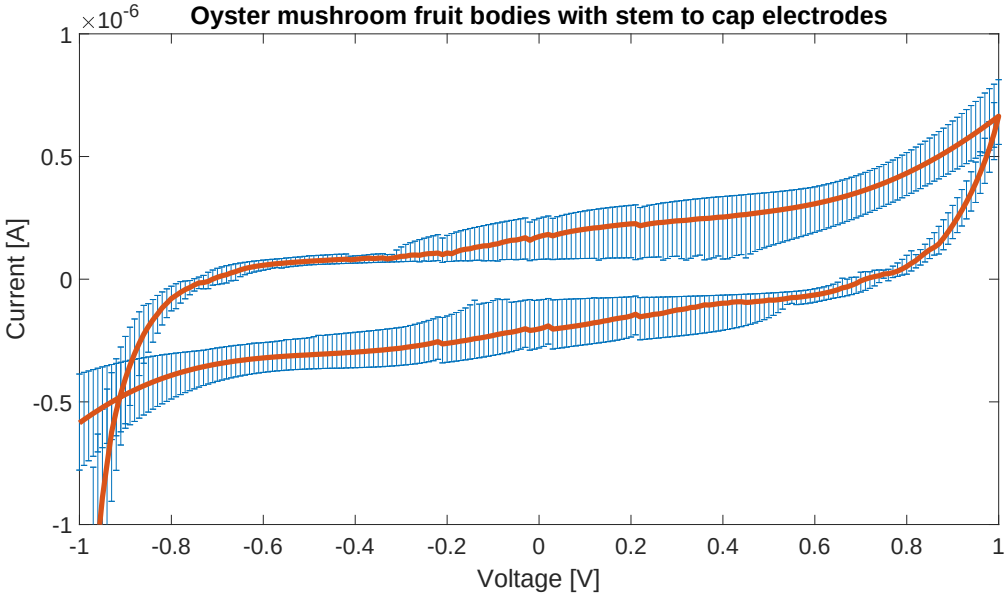

(b)

Figure 7. Average fruit bodies I-V characteristics for cyclic voltammetry of -1 V to 1 V. (a) Cap-to-cap electrode placement. (b) Stem-to-cap electrode placement.

behaviour.

Although the fruit bodies typically do not demonstrate the "pinching" property of an ideal memristor [52], it can be clearly seen that the biological matter exhibits memory properties when the electrical potential across the substrate is swept. A positive sweep yields a higher magnitude current when the applied voltage is positive; and a smaller

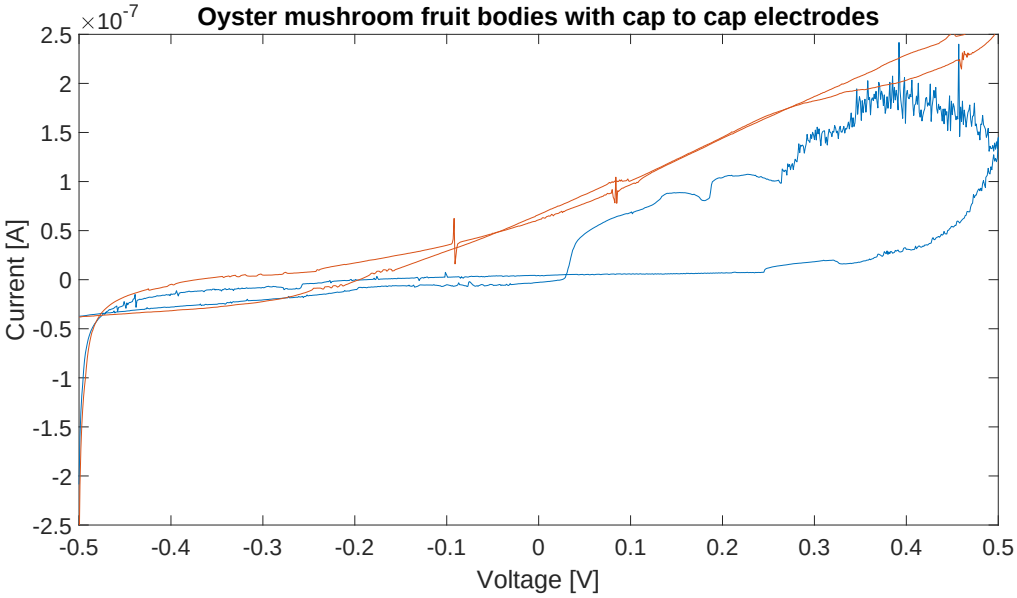

Figure 8. I-V Characteristics of fungi fruit bodies with the voltage step size set to 0.001 V. The two traces represent repeated runs of the same experiment.

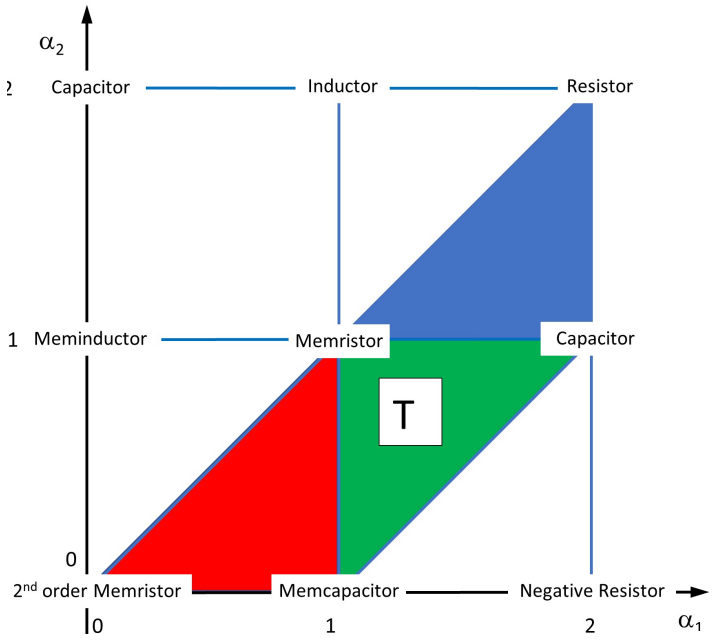

Figure 9. Principal memfractive elements

magnitude current when the applied voltage is negative.

Fractional Order Memory Elements (FOME) are proposed as a combination of Fractional Order Mem-Capacitors (FOMC) and Fractional Order Mem-Inductors (FOMI) [2]. The FOME (Eq. 1) is based on the generalised Ohm's law and parameterised as follows: α_1, α_2 are arbitrary real numbers — it is proposed that

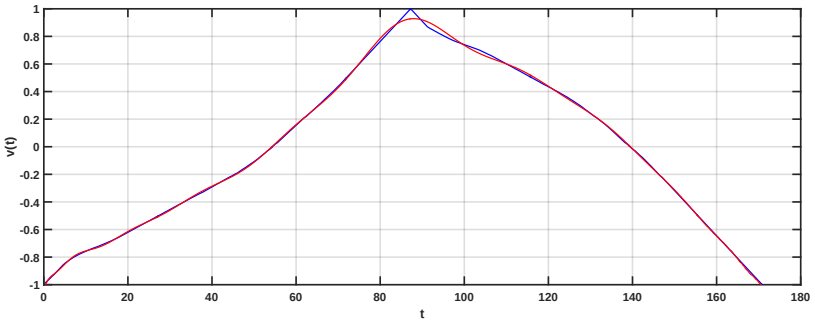

Figure 10. Voltage versus time and its approximation by a 24-degree polynomial

$0 \leq \alpha_1, \alpha_2 \leq 1$ models the solution space by [4], $F_M^{\alpha_1,\alpha_2}$ is the mem-fractance, $q(t)$ is the time dependent charge, $\varphi(t)$ is the time dependent flux. Therefore, the mem-fractance ($F_M^{\alpha_1,\alpha_2}$) is an interpolation between four points: MC — mem-capacitance, R_M — memristor, MI — mem-inductance, and $R_{2\,M}$ — the second order memristor (Fig. 9). Full derivations for the generalised FOME model are given by [2, 4]. The definition of mem-fractance can be straightforward generalised to any value of α_1, α_2 (see Fig. 27 in [2]).

$$D_t^{\alpha_1}\varphi(t) = F_M^{\alpha_1,\alpha_2}(t) D_t^{\alpha_2} q(t) \tag{1}$$

The appearance of characteristics from various memory elements in the fungal I-V curves supports the assertion that the fungal is a mem-fractor where α_1 and α_2 are both greater than 0 and less than 2.

There is no biological reason for mem-fractance of Oyster fungi fruit bodies with stem to cap electrodes, to be a usual closed formula. Therefore, one can get only a mathematical approximation of this function. In the following, we propose two alternatives to obtain the best approximation for mem-fractance in the case of average fruit bodies I-V characteristics for cyclic voltammetry of Fig. 7(b)

4.1. Approximation by polynomial on the whole interval of voltage

Raw data include the time, voltage and intensity of each reading. There are 171 readings for each run. The process of these data, in order to obtain a mathematical approximation of mem-fractance, in the first alternative, takes 4 steps as follows.

Step 1: approximate $v(t)$ by a twenty-four-degree polynomial (Fig. 10) whose coefficients are given in Table 1.

$$v(t) \approx P(t) = \sum_{j=0}^{j=24} a_j t^j \tag{2}$$

The polynomial fits very well the experimental voltage curve, as the statistical indexes show in Table 2.

Table 1. Coefficient of P(t)

a_0	-1.047361152400062	a_{13}	1.48292987584698e-16
a_1	0.135299293073760	a_{14}	-8.60157726907686e-19
a_2	-0.0726485498614107	a_{15}	1.59013702626457e-22
a_3	0.0240895989682110	a_{16}	5.80230108481181e-23
a_4	-0.00453232038841485	a_{17}	-7.12198496974121e-25
a_5	0.000531866967507868	a_{18}	5.19611819410190e-27
a_6	-4.19159536470121e-05	a_{19}	-2.64464369703488e-29
a_7	2.33484036114612e-06	a_{20}	9.68672841708898e-32
a_8	-9.51752589043893e-08	a_{21}	-2.52211206380669e-34
a_9	2.90458838155410e-09	a_{22}	4.45025298649318e-37
a_{10}	-6.72265349925510e-11	a_{23}	-4.78342788514078e-40
a_{11}	1.18302125464207e-12	a_{24}	2.36810109946699e-43
a_{12}	-1.56317950862153e-14		

Table 2. Goodness of fit

Sum of squared estimate of errors	$SSE = \sum_{j=1}^{j=n}(v_j - \hat{v}_j)^2$	0.0680517563652170
Sum of squared residuals	$SSR = \sum_{j=1}^{j=n}(\hat{v}_j - \overline{v})^2$	133.688517134422
Sum of square total	SST = SSE + SSR	133.756568890787
Coefficient of determination	$R-\text{square} = \frac{SSR}{SST}$	0.999491226809049

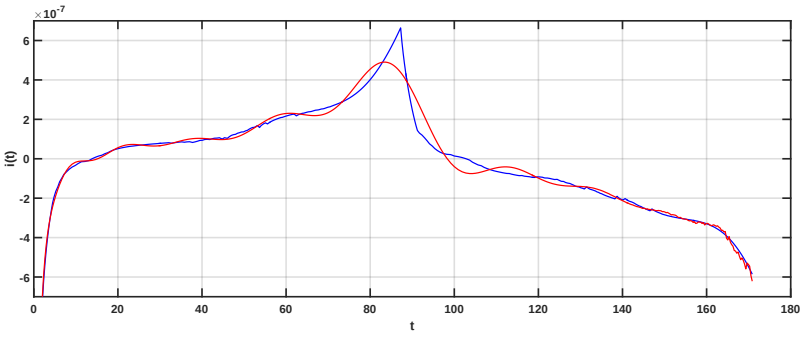

Figure 11. Current versus time and its approximation by a 24 degree polynomial

Step 2: in the same way approximate the current $i(t)$ using a twenty-four-degree polynomial (Fig. 11) whose coefficients are given in Table 3.

$$i(t) \approx Q(t) = \sum_{j=0}^{j=24} b_j t^j \tag{3}$$

Again, the polynomial fits well the experimental intensity curve, as displayed in Table 4.

Table 3. Coefficient of Q(t)

b_0	-2.69478636561017e-06	b_{13}	5.61870303550308e-22
b_1	1.95479195837707e-06	b_{14}	-3.66183256804588e-24
b_2	-7.34738169887512e-07	b_{15}	8.14484000064489e-27
b_3	1.67584032221916e-07	b_{16}	1.36036443304302e-28
b_4	-2.47326661661364e-08	b_{17}	-2.04593370725626e-30
b_5	2.48346182702953e-09	b_{18}	1.59708666114599e-32
b_6	-1.76692818009608e-10	b_{19}	-8.46294727047340e-35
b_7	9.19419585703268e-12	b_{20}	3.19831491989559e-37
b_8	-3.58289124918788e-13	b_{21}	-8.56384614589988e-40
b_9	1.06306849079070e-14	b_{22}	1.55262364796050e-42
b_{10}	-2.42471413376463e-16	b_{23}	-1.71535341852628e-45
b_{11}	4.25821973203331e-18	b_{24}	8.73846352218898e-49
b_{12}	-5.69947824465678e-20		

Table 4. Goodness of fit

Sum of squared estimate of errors	5.84247524503151e-13
Sum of squared residuals	4.07366051979587e-11
Sum of square total	4.13208527224619e-11
Coefficient of determination	0.985860709883522

Step 3: From (Eq. 1) used under the following form $D_t^{\alpha_2} q(t) \neq 0$.

$$F_M^{\alpha_1,\alpha_2}(t) = \frac{D_t^{\alpha_1}\varphi t}{D_t^{\alpha_2} q(t)} \tag{4}$$

and the Rieman-Liouville fractional derivative defined by [53].

$$ {}_0^{RL}D_t^{\alpha} f(t) = \frac{1}{\Gamma(m-\alpha)} \frac{d^m}{dt^m} \int_0^t (t-s)^{m-\alpha-1} f(s) ds, \text{ m - } 1 < \alpha < m \tag{5}$$

together with the formula for the power function

$$ {}_0^{RL}D_t^{\alpha} \left(at^{\beta}\right) = \frac{a\Gamma(\beta+1)}{\Gamma(\beta-\alpha+1)} t^{\beta-\alpha}, \ \beta > -1, \alpha > 0, \tag{6}$$

we obtain the closed formula of $F_M^{\alpha_1,\alpha_2}(t)$, approximation of the true biological mem-fractance of the Oyster mushroom

$$F_M^{\alpha_1,\alpha_2}(t) = \frac{D_t^{\alpha_1}\varphi(t)}{D_t^{\alpha_2}\varphi(t)} = \frac{{}_0^{RL}D_t^{\alpha_1} \sum_{j=0}^{j=24} \frac{a_j}{j+1} t^{j+1}}{{}_0^{RL}D_t^{\alpha_2} \sum_{j=0}^{j=24} \frac{b_j}{j+1} t^{j+1}} = \frac{\sum_{j=0}^{j=24} \frac{a_j \Gamma(j+1)}{\Gamma(j+2-\alpha_1)} t^{j+1-\alpha_1}}{\sum_{j=0}^{j=24} \frac{b_j \Gamma(j+1)}{\Gamma(j+2-\alpha_2)} t^{j+1-\alpha_2}} \tag{7}$$

Step 4: choice of parameter α_1 and α_2: We are looking for the best value of these parameters in the range $(\alpha_1, \alpha_2) \in [0,2]^2$. In this goal, we are considering first the singularities of $F_M^{\alpha_1,\alpha_2}(t)$ in order to avoid their existence, using suitable values of the

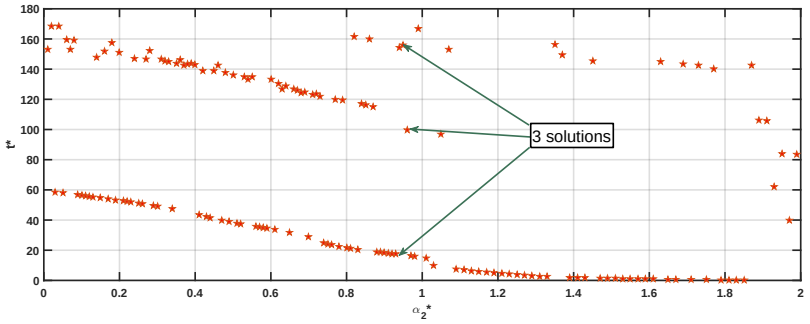

Figure 12. Zeros $t^*(\alpha_2)$ of the denominator of $F_M^{\alpha_1,\alpha_2}(t)$.

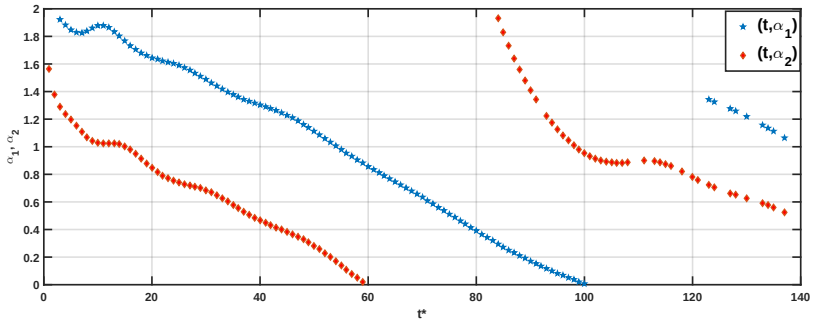

Figure 13. Zeros $t^*(\alpha_2)$ of $F_M^{\alpha_1,\alpha_2}(t)$ denominator (red dots), and zeros $t^*(\alpha_1)$ of the numerator (blue dots).

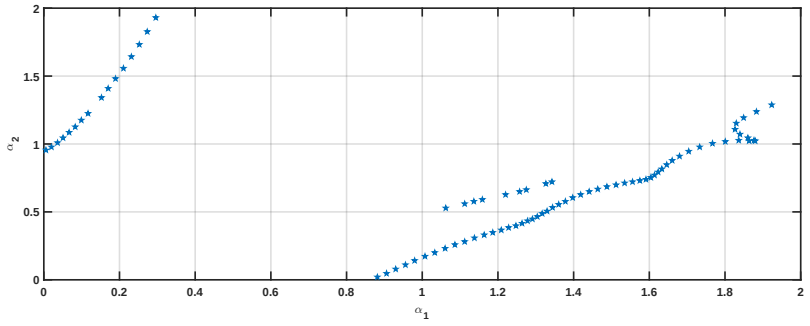

Figure 14. Values of $(\alpha_1, \alpha_2) \in [0, 2]^2$ for which the zeros $t^*(\alpha_2)$ of denominator of $F_M^{\alpha_1,\alpha_2}(t)$ correspond to the zeros $t^*(\alpha_1)$ of denominator.

parameters. Secondly, we will choose the most regular approximation. We compute numerically, the values $t^*(\alpha_2)$ which vanish the denominator of $F_M^{\alpha_1,\alpha_2}(t)$ (Fig. 12).

We observe one, two or three coexisting solutions depending on the value of α_2. Moreover, there is no value of α_2 without zero of the denominator. Therefore, in order to eliminate the singularities, we need to determine the couples $(\alpha_1, \alpha_2) \in [0, 2]^2$, vanishing simultaneously denominator and numerator of $F_M^{\alpha_1,\alpha_2}(t)$ (Figs. 13 and 14).

In the second part of step 4, we choose the most regular approximation. We consider that the most regular approximation is the one for which the function range $(F_M^{\alpha_1,\alpha_2}(t))$

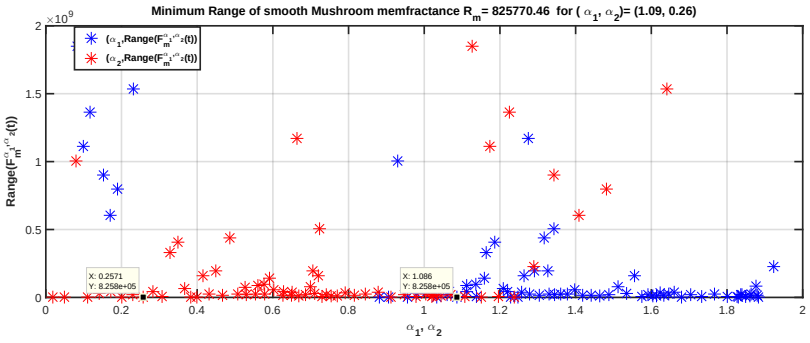

Figure 15. Values of range $(F_M^{\alpha_1,\alpha_2}(t))$ for $(\alpha_1, \alpha_2) \in [0,2]^2$

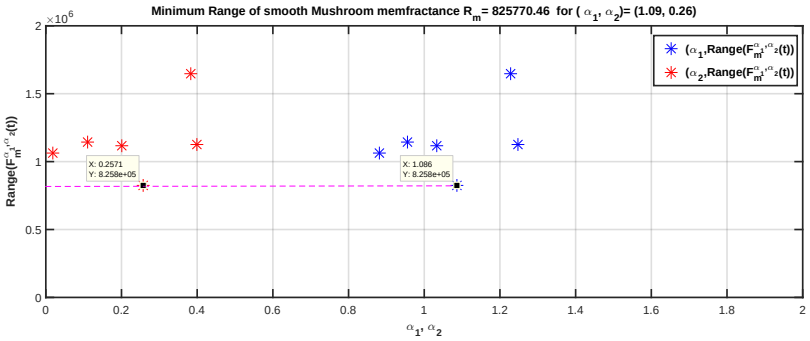

Figure 16. Magnification of Fig. 15.

Table 5. Minimum $F_M^{\alpha_1,\alpha_2}(t)$

α_1	α_2	**Minimum range** $F_M^{\alpha_1,\alpha_2}(t)$
1.08642731	0.25709492	825770.46017259

is minimal (Figs. 15 and 16).

$$\text{range}\left(F_M^{\alpha_1,\alpha_2}(t)\right) = \max_{t\in[0,171]}\left(F_M^{\alpha_1,\alpha_2}(t)\right) - \min_{t\in[0,171]}\left(F_M^{\alpha_1,\alpha_2}(t)\right) \quad (8)$$

From the numerical results, the best couple (α_1, α_2) and the minimum range of $F_M^{\alpha_1,\alpha_2}(t)$ are given in Table 5, and the corresponding Mem-fractance is displayed in Fig. 17.

The value of (α_1, α_2) given in Table 5 belongs to the triangle T of Fig. 9, whose vertices are Memristor, Memcapacitor and Capacitor. Which means that Oyster mushroom fruit bodies with stem to cap electrodes, is like a mix of such basic electronic devices.

As a counter-example of our method for choosing the best possible Mem-fractance, Fig. 18 displays, the Mem-fractance for a non-optimal couple $(\alpha_1, \alpha_2) = (1, 1.78348389322388)$ which presents two singularities.

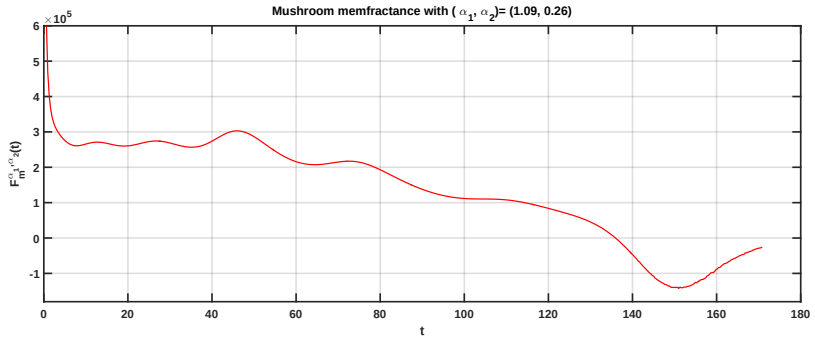

Figure 17. Mem-fractance for (α_1, α_2) given in Table 5.

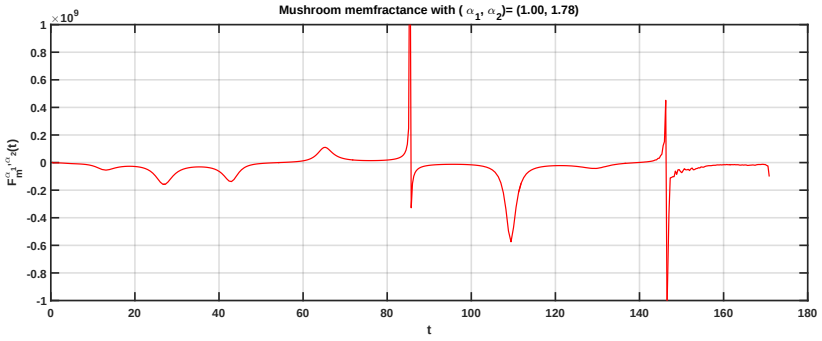

Figure 18. Mem-fractance with two singularities for $(\alpha_1, \alpha_2) = (1, 1.78348389322388)$.

4.2. Approximate cycling voltammetry

From the closed formula of $F_M^{\alpha_1^*,\alpha_2^*}(t)$ it is possible to retrieve the formula of the current function $i(t)$ using (Eq. 1).

$$
\begin{aligned}
i(t) &= D_t^{1-\alpha_2}\left[\frac{D_t^{\alpha_1}\varphi(t)}{F_M^{\alpha_1,\alpha_2}(t)}\right] \\
&= D_t^{1-\alpha_2}\left[\frac{\sum_{j=0}^{j=24}\frac{a_j\Gamma(j+1)}{\Gamma(j+2-\alpha_1)}t^{j+1-\alpha_1}}{\frac{\sum_{j=0}^{j=24}\frac{a_j\Gamma(j+1)}{\Gamma(j+2-\alpha_1)}t^{j+1-\alpha_1}}{\sum_{j=0}^{j=24}\frac{b_j\Gamma(j+1)}{\Gamma(j+2-\alpha_2)}t^{j+1-\alpha_2}}}\right] \\
&= D_t^{1-\alpha_2}\left[\sum_{j=0}^{j=24}\frac{b_j\Gamma(j+1)}{\Gamma(j+2-\alpha_2)}t^{j+1-\alpha_2}\right] \\
&= \sum_{j=0}^{j=24}\frac{\Gamma(j+2-\alpha_2)b_j\Gamma(j+1)}{\Gamma(j+2-\alpha_2)\Gamma(j+1)}t^{j+1-\alpha_2-(1-\alpha_2)} \\
&= \sum_{j=0}^{j=24} b_j t^j
\end{aligned}
\tag{9}
$$

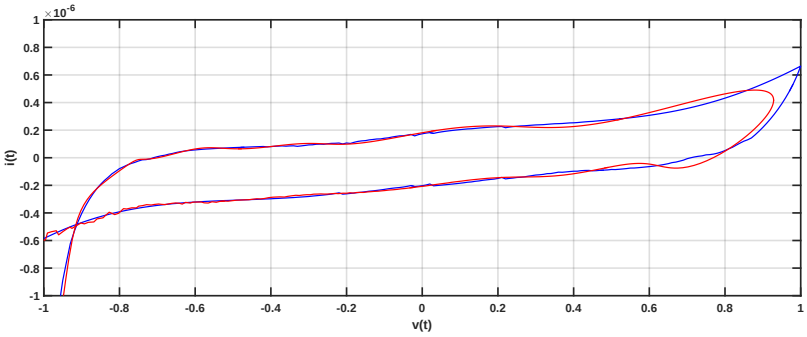

Figure 19. Comparison between average experimental data of cyclic voltammetry performed over -1 V to 1 V, Stem-to-cap electrode placement, and approximate values of $v(t)$ and $i(t)$.

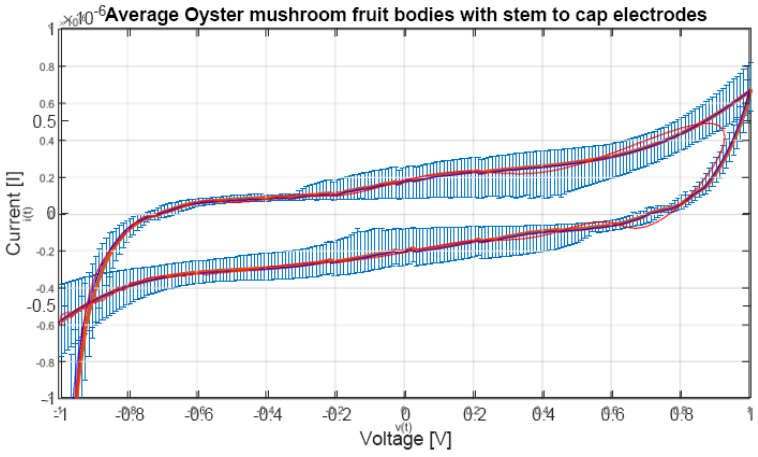

Figure 20. Both average experimental data curve and the curve computed from closed approximative formula are nested into the histogram of data of all runs.

The comparison of average experimental data of cyclic voltammetry performed over -1 V to 1 V, stem-to-cap electrode placement, and closed approximative formula is displayed in Fig. 19, showing a good agreement between both curves except near the maximum value of $v(t)$ and $i(t)$. Figure 20 shows that the curve computed from closed approximative formula belongs to the histogram of data of all runs. The discrepancy between both curves is due to the method of approximation chosen in (2) and (3).

It is possible, as we show in the next subsection to improve the fitting of the approximated curve near the right hand-side vertex, using piecewise polynomial approximation of both $v(t)$ and $i(t)$.

4.3. Alternative approximation of the cycling voltammetry

Due to the way of conducting the experiments, the voltage curve presents a vertex, that means that the function $v(t)$ is non-differentiable for $T = 87.23747459$. In fact, the

Table 6. Coefficient for i(t)

Coefficient	Value for $0 \leq t \leq T$	Coefficient	Value for $T \leq t < T$
a_0	-0.98299	a'_0	37.16955
a_1	0.02665	a'_1	-1.2986
a_2	-5.91565 E -4	a'_2	0.01826
a_3	1.12211 E -5	a'_3	-1.25146 E -4
a_4	-6.28483 E -8	a'_4	4.12302 E -7
a_5	6.9675 E -11	a'_5	-5.25359 E-19

Table 7. Goodness of fit

Approximation	$t < T$	$t > T$
Coefficient of determination	0.99983	0.9999

value of T is the average value of the non-differentiable points for the 20 runs.

In this alternative approximation, we follow the same 4 steps as previously, changing the approximation by a twenty-four-degree polynomial to an approximation by a 2-piecewise fifth-degree-polynomial, for both $v(t)$ and $i(t)$.

Step 1: approximation of $v(t)$ by a 2-piecewise fifth-degree-polynomial (Fig. 21) whose coefficients are given in Table 6.

$$v(t) = \begin{cases} P_1(t) = & a_0 + a_1 t + a_2 t^2 + a_3 t^3 \\ & + a_4 t^4 + a_5 t^5, \text{ for } 0 \leq t \leq T \\ P_2(t) = & a'_0 + a'_1 t + a'_2 t^2 + a'_3 t^3 \\ & + a'_4 t^4 + a'_5 t^5, \text{ for T} \leq t < 171 \end{cases} \tag{10}$$

The flux is obtained integrating $v(t)$ versus time. The polynomial fits very well the experimental voltage curve, as the statistical indexes show in Table 7.

$$\varphi(t) = \begin{cases} IP_1(t) = & a_0 t + \frac{a_1}{2} t^2 + \frac{a_2}{3} t^3 + \frac{a_3}{4} t^4 \\ & + \frac{a_4}{5} t^5 + \frac{a_5}{6} t^6, \text{ for } 0 \leq t \leq T \\ IP_2(t) = & a'_0 t + \frac{a'_1}{2} t^2 + \frac{a'_2}{3} t^3 + \frac{a'_3}{4} t^4 \\ & + \frac{a'_4}{5} t^5 + \frac{a'_5}{6} t^6, \text{ for } T \leq t < 171 \end{cases} \tag{11}$$

Step 2: in the same way, one approximates the current $i(t)$ using a 2-piecewise

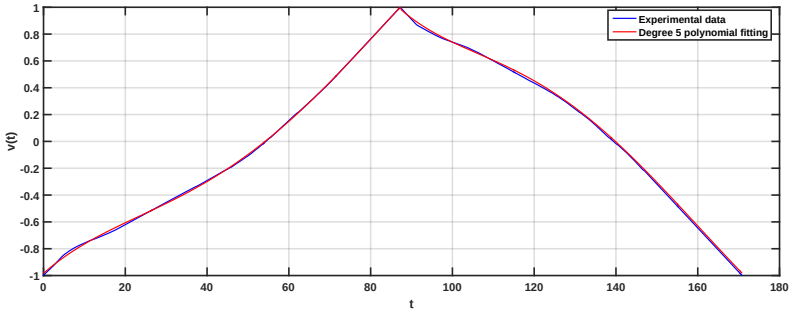

Figure 21. Voltage versus time and its approximation by 2-piecewise fifth degree polynomial

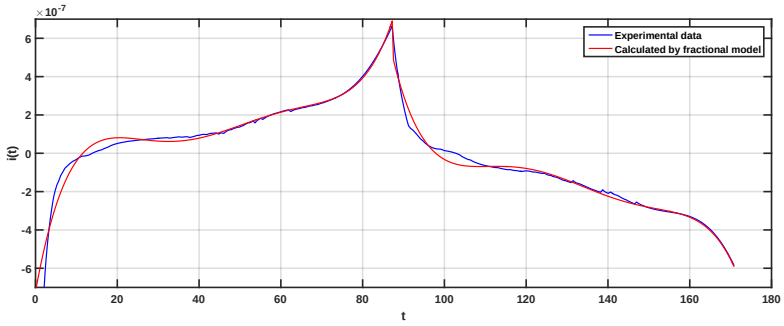

Figure 22. Current versus time and its approximation by 2-piecewise fifth degree polynomial

fifth degree polynomial (Fig. 22) whose coefficients are given in Table 8.

$$i(t) = \begin{cases} P_3(t) = & b_0 + b_1 t + b_2 t^2 + b_3 t^3 \\ & + b_4 t^4 + b_5 t^5, \text{ for } 0 \leq t \leq T \\ P_4(t) = & b'_0 + b'_1 t + b'_2 t^2 + b'_3 t^3 \\ & + b'_4 t^4 + b'_5 t^5, \text{ for } T \leq t < 171 \end{cases} \tag{12}$$

Again, the polynomial fits very well the experimental voltage curve, as the statistical indexes show in Table 9. Therefore, the charge is given by:

$$q(t) = \begin{cases} IP_3(t) = & b_0 t + \frac{b_1}{2} t^2 + \frac{b_2}{3} t^3 + \frac{b_3}{4} t^4 \\ & + \frac{b_4}{5} t^5 + \frac{b_5}{6} t^6, \text{ for } 0 \leq t \leq T \\ IP_4(t) = & b'_0 t + \frac{b'_1}{2} t^2 + \frac{b'_2}{3} t^3 \\ & + \frac{b'_3}{4} t^4 + \frac{b'_4}{5} t^5 + \frac{b'_5}{6} t^6, \text{ for } T \leq t < 171 \end{cases} \tag{13}$$

Table 8. Coefficient for i(t)

Coefficient	Value for $0 \leq t \leq T$	Coefficient	Value for $T \leq t < 171$
b_0	-7.21418 E -7	b'_0	2.69466 E -4
b_1	1.11765 E -7	b'_1	-1.05461 E -5
b_2	-6.3792 E -9	b'_2	1.63678 E -7
b_3	1.57327 E -10	b'_3	-1.25915 E -9
b_4	-1.7745 E -12	b'_4	4.80107 E -12
b_5	7.52304 E -15	b'_5	-7.26253 E-15

Table 9. Goodness of fit

Approximation	$t < T$	$t > T$
Coefficient of determination	0.99171	0.98613

Step 3: Following the same calculus as before with (4), one obtains:

$$\text{for } 0 \leq t \leq T,\ F_M^{\alpha_1,\alpha_2}(t) = \frac{{}_0^{RL}D_t^{\alpha_1}\varphi(t)}{{}_0^{RL}D_t^{\alpha_2}q(t)} = \frac{{}_0^{RL}D_t^{\alpha_1}[IP_1(t)]}{{}_0^{RL}D_t^{\alpha_2}[IP_3(t)]} = \frac{\sum_{j=1}^{j=5}\frac{a_j\Gamma(j+1)}{\Gamma(j+2-\alpha_1)}t^{j+1-\alpha_1}}{\sum_{j=0}^{j=5}\frac{b_j\Gamma(j+1)}{\Gamma(j+2-\alpha_2)}t^{j+1-\alpha_2}} \tag{14}$$

However, because fractional derivative has memory effect, for $T < t < 171$, the formula is slightly more complicated (depicted in Eq. 15).

Using integration by part repeatedly six times we obtain Eq. 16. In this 2-piece wise approximation, the vertex is non-differentiable, this implies that Eq. 16 expression has a singularity at T (because $(t-T)^{-\alpha_{1,2}} \to \infty$). It could be possible to avoid this singularity, using a 3-piece wise approximation, smoothing the vertex. However, the calculus are very tedious. We will explain, below, what our simpler choice implies. Finally, Eqs. 17 and 18 are obtained.

$$
\begin{aligned}
F_M^{\alpha_1,\alpha_2}(t) &= \frac{{}_0^{RL}D_t^{\alpha_1}\varphi(t)}{{}_0^{RL}D_t^{\alpha_2}q(t)} \qquad (15)\\
&= \frac{\frac{1}{\Gamma(m_1-\alpha_1)}\frac{d^{m_1}}{dt^{m_1}}\int_0^t (t-s)^{m_1-\alpha_1-1}\varphi(s)ds}{\frac{1}{\Gamma(m_2-\alpha_2)}\frac{d^{m_2}}{dt^{m_2}}\int_0^t (t-s)^{m_2-\alpha_2-1}q(s)ds},\ m_1-1<\alpha_1<m_1 \text{ and } m_2-1<\alpha_2<m_2\\
&= \frac{\frac{1}{\Gamma(m_1-\alpha_1)}\frac{d^{m_1}}{dt^{m_1}}\left[\int_0^T (t-s)^{m_1-\alpha_1-1}IP_1(s)ds+\int_T^t (t-s)^{m_1-\alpha_1-1}IP_2(s)ds\right]}{\frac{1}{\Gamma(m_2-\alpha_2)}\frac{d^{m_2}}{dt^{m_2}}\left[\int_0^T (t-s)^{m_2-\alpha_2-1}IP_3(s)ds+\int_T^t (t-s)^{m_2-\alpha_2-1}IP_4(s)ds\right]}\\
&= \frac{\frac{1}{\Gamma(m_1-\alpha_1)}\frac{d^{m_1}}{dt^{m_1}}\sum_{j=0}^{j=5}\left[\frac{a_j}{j+1}\int_0^T (t-s)^{m_1-\alpha_1-1}s^{j+1}ds+\frac{a'_j}{j+1}\int_T^t (t-s)^{m_1-\alpha_1-1}s^{j+1}ds\right]}{\frac{1}{\Gamma(m_2-\alpha_2)}\frac{d^{m_2}}{dt^{m_2}}\sum_{j=0} j=5\left[\frac{b_j}{j+1}\int_0^T (t-s)^{m_2-\alpha_2-1}s^{j+1}ds+\frac{b'_j}{j+1}\int_T^t (t-s)^{m_2-\alpha_2-1}s^{j+1}ds\right]}
\end{aligned}
$$

$$
\begin{aligned}
&F_M^{\alpha_1,\alpha_2}(t) \qquad (16)\\
&= \frac{\frac{1}{\Gamma(m_1-\alpha_1)}\frac{d^{m_1}}{dt^{m_1}}\sum_{j=0}^{j=5}\left[\frac{a_j}{j+1}\left[\sum_{k=0}^{k=j+1}\left[\frac{-(j+1)!\Gamma(m_1-\alpha_1)(t_T)^{m_1+k-\alpha_1}T^{j+1-k}}{(j+1-k)!\Gamma(m_1+k+1-\alpha_1}\right]+\frac{(j+1)!\Gamma(m_1-\alpha_1)t^{m_1+k-\alpha_1}}{\Gamma(m_1+j+1-\alpha_1)}\right]+\frac{a'_j}{j+1}\left[\sum_{k=0}^{k=j+1}\frac{(j+1)!\Gamma(m_1-\alpha_1)(t-T)^{m_1+k-\alpha_1}T^{j+1-k}}{(j+1-k)!\Gamma(m_1+k+1-\alpha_1)}\right]\right]}{\frac{1}{\Gamma(m_2-\alpha_2)}\frac{d^{m_2}}{dt^{m_2}}\sum_{j=0}^{j=5}\left[\frac{b_j}{j+1}\left[\sum_{k=0}^{k=j+1}\left[\frac{-(j+1)!\Gamma(m_2-\alpha_2)(t-T)^{m_2+k-\alpha_2}T^{j+1-k}}{(j+1-k)!\Gamma(m_2+k+1-\alpha_2)}\right]+\frac{(j+1)!\Gamma(m_2-\alpha_2)t^{m_2+k-\alpha_2}}{\Gamma(m_2+j+1-\alpha_2)}\right]+\frac{b'_j}{j+1}\left[\sum_{k=0}^{k=j+1}\frac{(j+1)!\Gamma(m_2-\alpha_2)(t-T)^{m_2+k-\alpha_2}T^{j+1-k}}{(j+1-k)!\Gamma(m_2+k+1-\alpha_2)}\right]\right]}\\
&= \frac{\frac{1}{\Gamma(m_1-\alpha_1)}\frac{d^{m_1}}{dt^{m_1}}\sum_{j=0}^{j=5}\left[(a'_j-a_j)\sum_{k=0}^{k=j+1}\left[\frac{j!\Gamma(m_1-\alpha_1)(t-T)^{m_1+k-\alpha_1}T^{j+1-k}}{(j+1-k)!\Gamma(m_1+k+1-\alpha_1)}\right]+a_j\frac{j!\Gamma(m_1-\alpha_1)t^{m_1+j+1-\alpha_1}}{\Gamma(m_1+j+2-\alpha_1}\right]}{\frac{1}{\Gamma(m_2-\alpha_2)}\frac{d^{m_2}}{dt^{m_2}}\sum_{j=0}^{j=5}\left[(b'_j-b_j)\sum_{k=0}^{k=j+1}\left[\frac{j!\Gamma(m_2-\alpha_2)(t-T)^{m_2+k-\alpha_2}T^{j+1-k}}{(j+1-k)!\Gamma(m_2+k+1-\alpha_2)}\right]+b_j\frac{j!\Gamma(m_2-\alpha_2)t^{m_2+j+1-\alpha_2}}{\Gamma(m_2+j+2-\alpha_2)}\right]}\\
&= \frac{\sum_{j=0}^{j=5}\left[(a'_j-a_j)\sum_{k=0}^{k=j+1}\left[\frac{j!(t-T)^{k-\alpha_1}T^{j+1-k}}{(j+1-k)!\Gamma(k+1-\alpha_1)}\right]+a_j\frac{j!t^{j+1-\alpha_1}}{\Gamma(j+2-\alpha_1)}\right]}{\sum_{j=0}^{j=5}\left[(b'_j-b_j)\sum_{k=0}^{k=j+1}\left[\frac{j!(t-T)^{k-\alpha_2}T^{j+1-k}}{(j+1-k)!\Gamma(k+1-\alpha_2)}\right]+b_j\frac{j!t^{j+1-\alpha_2}}{\Gamma(j+2-\alpha_2)}\right]}
\end{aligned}
$$

$$
\begin{aligned}
F_M^{\alpha_1,\alpha_2}(t) &= \frac{(t-T)^{-\alpha_1}\left[\sum_{j=0}^{j=5}\left[\left(a'_j-a_j\right)\sum_{k=0}^{k=j+1}\left[\frac{j!(t-T)^{k}T^{j+1-k}}{(j+1-k)!\Gamma(k+1-\alpha_1)}\right]+a_j\frac{j!t^{j+1-\alpha_1}(t-T)^{\alpha_1}}{\Gamma(j+2-\alpha_1)}\right]\right]}{(t-T)^{-\alpha_2}\left[\sum_{j=0}^{j=5}\left[\left(b'_j-b_j\right)\sum_{k=0}^{k=j+1}\left[\frac{j!(t-T)^{k}T^{j+1-k}}{(j+1-k)!\Gamma(k+1-\alpha_2)}\right]+b_j\frac{j!t^{j+1-\alpha_2}(t-T)^{\alpha_2}}{\Gamma(j+2-\alpha_2)}\right]\right]} \\
&= \frac{\sum_{j=0}^{j=5}\left[\left(a'_j-a_j\right)\sum_{k=0}^{k=j+1}\left[\frac{j!(t-T)^{k}T^{j+1-k}}{(j+1-k)!\Gamma(k+1-\alpha_1)}\right]+a_j\frac{j!t^{j+1-\alpha_1}(t-T)^{\alpha_1}}{\Gamma(j+2-\alpha_1)}\right]}{(t-T)^{\alpha_1-\alpha_2}\sum_{j=0}^{j=5}\left[\left(b'_j-b_j\right)\sum_{k=0}^{k=j+1}\left[\frac{j!(t-T)^{k}T^{j+1-k}}{(j+1-k)!\Gamma(k+1-\alpha_2)}\right]+b_j\frac{j!t^{j+1-\alpha_2}(t-T)^{\alpha_2}}{\Gamma(j+2-\alpha_2)}\right]}
\end{aligned}
\tag{17}
$$

$$
F_M^{\alpha_1,\alpha_2}(t) = \begin{cases} \dfrac{\sum_{j=0}^{j=5}\frac{a_j\Gamma(j+1)}{\Gamma(j+2-\alpha_1)}t^{j+1-\alpha_1}}{\sum_{j=0}^{j=5}\frac{b_j\Gamma(j+1)}{\Gamma(j+2-\alpha_2)}t^{j+1-\alpha_2}}, & \text{for} \quad 0 \le t \le T \\ \dfrac{\sum_{j=0}^{j=5}\left[\left(a'_j-a_j\right)\sum_{k=0}^{k=j+1}\left[\frac{j!(t-T)^{k}T^{j+1-k}}{(j+1-k)!\Gamma(k+1-\alpha_1)}\right]+a_j\frac{j!t^{j+1-\alpha_1}(t-T)^{\alpha_1}}{\Gamma(j+2-\alpha_1)}\right]}{(t-T)^{\alpha_1-\alpha_2}\sum_{j=0}^{j=5}\left[\left(b'_j-b_j\right)\sum_{k=0}^{k=j+1}\left[\frac{j!(t-T)^{k}T^{j+1-k}}{(j+1-k)!\Gamma(k+1-\alpha_2)}\right]+b_j\frac{j!t^{j+1-\alpha_2}(t-T)^{\alpha_2}}{\Gamma(j+2-\alpha_2)}\right]}, & \text{for} \quad T < t < 171 \end{cases}
\tag{18}
$$

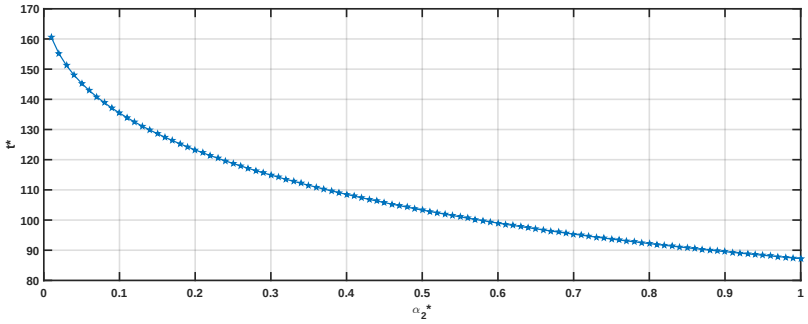

Figure 23. The first zero $t^*(\alpha_2) \geq T$, of the denominator of $F_M^{\alpha_1,\alpha_2}(t)$, as function of α_2.

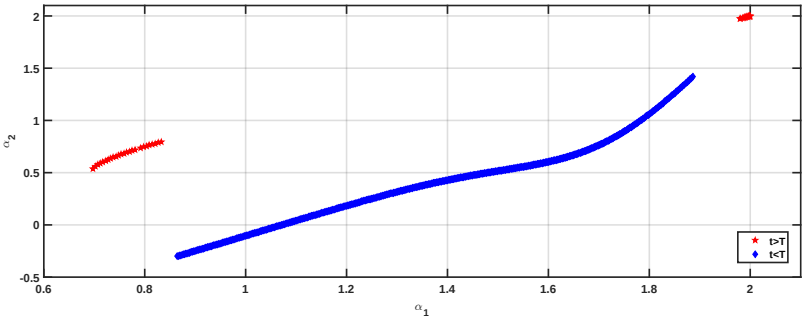

Figure 24. Couples (α_1, α_2) for which the denominator and numerator of $F_M^{\alpha_1,\alpha_2}(t)$ are null simultaneously for $t < T$ (blue dot) and $t > T$ (red dot).

Step 4: choice of parameter α_1 and α_2: Following the same idea as for the first alternative, we try to avoid singularity for $F_M^{\alpha_1,\alpha_2}(t)$, except of course the singularity near T, which is of mathematical nature (non-differentiability of voltage and intensity at $t = T$). Figure 23 displays the first zero $t^*(\alpha_2) \geq T$, of the denominator of $F_M^{\alpha_1,\alpha_2}(t)$. One can see that $t^*(1) \cong T$.

Figure 24 displays the curves of couples (α_1, α_2) for which the denominator and numerator of $F_M^{\alpha_1,\alpha_2}(t)$ are null simultaneously for $t < T$ and $t > T$. On this figure, the value of α_1, that corresponds to $\alpha_2 = 1$ is $\alpha_1 \approx 1.78348389322388$. The corresponding Mem-fractance is displayed in Fig. 25.

The singularity observed in Figs. 25 and 26 is due to the non-differentiability of both voltage and intensity functions at point T. It is only a mathematical problem of approximation which can be solved using a 3-piecewise polynomial instead of the 2-piecewise polynomial $(P1(t),\ P2(t))$ and $(P3(t),\ P4(t))$. The third added piecewise polynomials for $v(t)$ and $i(t)$ being defined on the tiny interval [87.24, 87.90]. However due to more tedious calculus, we do not consider this option in the present study. It is only a math problem, and one can consider that Fig. 28 represents the value of the mem-fractance in the interval $[0, 87.24] \cup [87.90, 171]$.

The value of $(\alpha_1 = 1.78, \alpha_2 = 1.00)$ belongs to the line segment of Fig. 9, whose

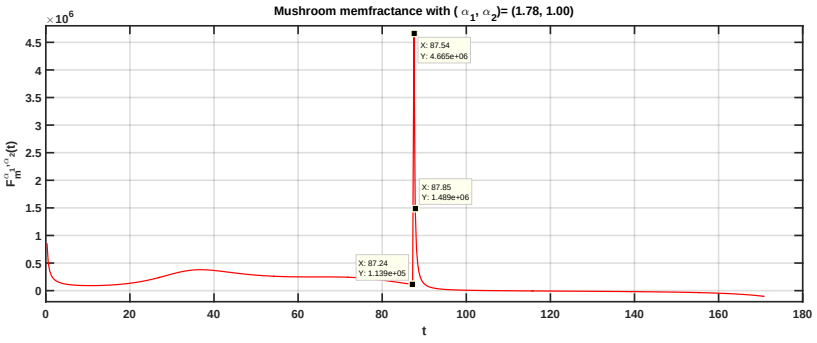

Figure 25. Mem-fractance for $(\alpha_1 = 1.78, \alpha_2 = 1.00)$ given in Table 5

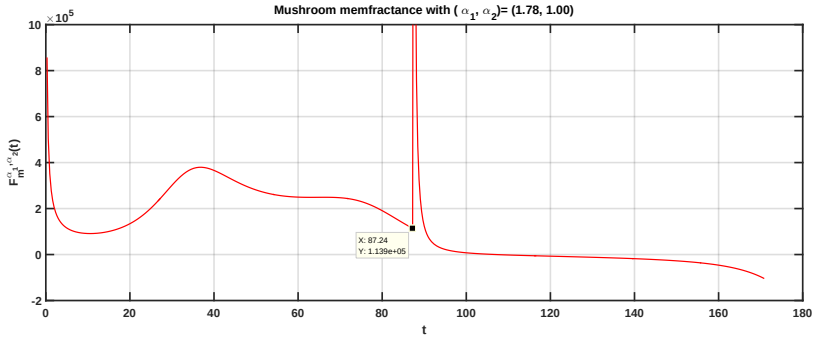

Figure 26. Magnification of Fig. 25

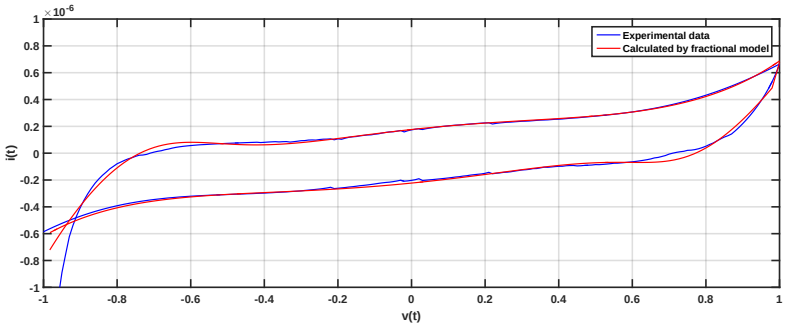

Figure 27. Comparison between average experimental data of cyclic voltammetry performed over -1 V to 1 V, Stem-to-cap electrode placement, and closed approximative formula.

extremities are Memristor, and Capacitor. Which means that Oyster mushroom fruit bodies with stem-to-cap electrodes, is like a mix of such basic electronic devices. The comparison of average experimental data of cyclic voltammetry performed over -1 V to 1 V, stem-to-cap electrode placement, and closed approximative formula is displayed in Fig. 27, showing a very good agreement between both curves.

5. Discussion

Two are the main remarks of this study. First, both approximations used in Section 4 converge to Mem-fractance with parameter value (α_1, α_2) - belonging inside or on edge of the triangle T of Fig. 9, whose vertices are Memristor, Memcapacitor and Capacitor. Of course, the value for these approximations are not exactly the same. This is in part, due to the fact that we consider that the most regular approximation is the one for which the function range $(F_M^{\alpha_1,\alpha_2}(t))$ is minimal. Other choices based on physiology of Mushroom could be invoked. Moreover, the Mem-fractance is computed on the averaged curve of 20 runs which do not present exactly the same characteristic voltammetry. Oyster mushroom fruit bodies are living substrates. Commonly for living substrates their morphology, i.e. geometry of the translocation zones [50], is changing from one fruit body to another. This high variability prevents exact reproduction of electrical property between the experimental trials.

The second remark is the fact that the use of fractional derivatives to analyze the mem-fractance, is obvious if one considers that fractional derivatives have memory, which allows a perfect modelling of memristive elements. Their handling is however delicate if one wants to avoid any flaw.

Similar I-V characteristics have been experienced for slime mould [15] and apples [13]. The cyclic voltammetry experiments demonstrate that the I-V curve produced from these living substrates is a closed loop where the negative path does not match the positive path. Hence the fungi display the characteristics of a memristor. A similar conclusion is drawn for the microtubule experiments [54]. The microtubule exhibits different resistive properties for the same applied voltage depending on the history of applied voltages.

Additionally, the fruit bodies produce current oscillations during the cyclic voltammetry. This oscillatory effect is only observed on one phase of the voltammetry for a given voltage range which is, again, a behaviour that can be associated to a device whose resistance is a function of its previous resistance. This spiking activity is typical of a device that exhibits memristive behaviours. Firstly, it was reported in experiments with electrochemical devices using graphite reference electrodes, that a temporal dependence of the current of the device - at constant applied voltage - causes charge accumulation and discharge [55]. The spiking is also apparent in some plots, for a large electrode size, in experiments with electrode metal on solution-processed flexible titanium dioxide memristors [56]. A detailed analysis of types of spiking emerging in simulated memristive networks was undertaken in [57]. Repeatable observations of the spiking behaviour in I-V of the fungi is very important because this opens new pathways for the implementation of neuromorphic computing with fungi. A fruitful theoretical foundation of this field is already well developed [58, 59, 60, 61, 62, 63].

6. Conclusion

The fruit bodies of grey oyster fungi *Pleurotus ostreatus* were subjected to I-V characterisation a number of times, from which it was clearly shown that they exhibit mem-fractor properties. Under cyclic voltammetry, the fruit body will conduct differently depending on the phase (positive or negative) of the voltammetry. This behaviour produces the classic "lobes" in the I-V characteristics of a memristor.

However, a biological medium, such as the fruit body of the grey Oyster fungi presented here, will differ from that of the ideal memristor model since the "pinching" behaviour and size of the hysteresis lobes are functions of the frequency of the voltage sweep as well as the previous resistance. Typically, the biological medium generates its own potential across the electrodes, therefore, even when no additional potential is supplied, there is still current flow between the probes. This property of the fungi produces an opening in the I-V curve that is a classic property of the mem-capacitor. Since the fungi are exhibiting properties of both memristors and mem-capacitors, their electrical memory behaviour puts them somewhere in the mem-fractor solution space where $0 < \alpha_1, \alpha_2 < 1$. Hence, it has been shown that fungi act as mem-fractors.

We believe a potential practical implementation of the mem-fractive properties of the fungi would be in the sensorial and computing circuits embedded into mycelium bound composites. In [24] we proposed to develop a structural substrate by using live fungal mycelium, functionalise the substrate with nanoparticles and polymers to make mycelium-based electronics, implement sensorial fusion and decision making in the mycelium networks [64] and to grow monolithic buildings from the functionalised fungal substrate [65]. Fungal buildings would self-grow, build, and repair themselves subject to substrate supplied, use natural adaptation to the environment, sense all that humans can sense. Whilst major parts of a building will be made from dried and cured mycelium composites there is an opportunity to use blocks with living mycelium as embedded living computing elements. Right now we established just some components of the computing fungal architectures. Future challenges will be in implementation of a large scale computing circuits employing mem-fractive properties of the living mycelium and fruit bodies and an integration of living mycelium computers into buildings made from biomaterials.

Acknowledgement

This project has received funding from the European Union's Horizon 2020 research and innovation programme FET OPEN "Challenging current thinking" under grant agreement No 858132.

References

[1] Chua L 1971 *IEEE Transactions on Circuit Theory* **18** 507–519 ISSN 2374-9555

[2] Abdelouahab M S, Lozi R and Chua L 2014 *International Journal of Bifurcation and Chaos* **24** 1430023

[3] Strukov D B, Snider G S, Stewart D R and Williams R S 2008 *Nature* **453** 80–83 ISSN 0028-0836

[4] Khalil N A, Said L A, Radwan A G and Soliman A M 2019 *Microelectronics Journal* **90** 211–221

[5] Ginoux J M and Rossetto B 2013 The singing arc: the oldest memristor? *Chaos, CNN, Memristors and Beyond: A Festschrift for Leon Chua With DVD-ROM, composed by Eleonora Bilotta* (World Scientific) pp 494–507

[6] Erokhin V, Berzina T and Fontana M P 2005 *Journal of applied physics* **97** 064501

[7] Martinsen Ø G, Grimnes S, Lütken C and Johnsen G 2010 *Journal of Physics: Conference Series* **224** 012071

[8] Pabst O, Martinsen Ø G and Chua L 2018 *Scientific reports* **8** 1–9

[9] Pabst O, Martinsen Ø G and Chua L 2019 *Scientific reports* **9** 1–10

[10] Kosta S P, Kosta Y P, Bhatele M, Dubey Y, Gaur A, Kosta S, Gupta J, Patel A and Patel B 2011 *International Journal of Medical Engineering and Informatics* **3** 16–29

[11] Volkov A G, Tucket C, Reedus J, Volkova M I, Markin V S and Chua L 2014 *Plant signaling & behavior* **9** e28152

[12] Volkov A G and Chua L 2021 *Functional Plant Biology* **48** 567–572

[13] Volkov A G and Markin V S 2017 *Russian Journal of Electrochemistry* **53** 1011–1018 ISSN 1023-1935

[14] Abdelrahman D K, Mohammed R, Fouda M E, Said L A and Radwan A G 2021 *IEEE Access* **9** 21498–21506

[15] Gale E, Adamatzky A and de Lacy Costello B 2015 *BioNanoScience* **5** 1–8

[16] Braund E and Miranda E R 2017 *Journal of Bionic Engineering* **14** 151–162

[17] del Rocío Cantero M, Perez P L, Scarinci N and Cantiello H F 2019 *Scientific reports* **9** 1–10

[18] Chiolerio A, Draper T C, Mayne R and Adamatzky A 2020 *Journal of colloid and interface science* **560** 589–595

[19] Tuszynski J A, Friesen D, Freedman H, Sbitnev V I, Kim H, Santelices I, Kalra A P, Patel S D, Shankar K and Chua L O 2020 *Scientific reports* **10** 1–11

[20] More G M, Tiwari A P, Pawar K D, Dongale T D and Kim T G 2021 Bipolar resistive switching in biomaterials: case studies of dna and melanin-based bio-memristive devices *Mem-elements for Neuromorphic Circuits with Artificial Intelligence Applications* (Elsevier) pp 299–323

[21] Sun B, Guo T, Zhou G, Wu J, Chen Y, Zhou Y N and Wu Y A 2021 *ACS Applied Bio Materials* **4** 1976–1985

[22] Adamatzky A 2018 *Scientific reports* **8** 1–7

[23] Adamatzky A 2018 *Interface focus* **8** 20180029

[24] Adamatzky A, Ayres P, Belotti G and Wosten H 2019 *arXiv preprint arXiv:1912.13262*

[25] Borghetti J, Snider G S, Kuekes P J, Yang J J, Stewart D R and Williams R S 2010 *Nature* **464** 873–876

[26] Kvatinsky S, Satat G, Wald N, Friedman E G, Kolodny A and Weiser U C 2013 *IEEE Transactions on Very Large Scale Integration (VLSI) Systems* **22** 2054–2066

[27] Linn E, Rosezin R, Tappertzhofen S, Böttger U and Waser R 2012 *Nanotechnology* **23** 305205

[28] Kvatinsky S, Belousov D, Liman S, Satat G, Wald N, Friedman E G, Kolodny A and Weiser U C 2014 *IEEE Transactions on Circuits and Systems II: Express Briefs* **61** 895–899

[29] Borghetti J, Li Z, Straznicky J, Li X, Ohlberg D A, Wu W, Stewart D R and Williams R S 2009 *Proceedings of the National Academy of Sciences* **106** 1699–1703

[30] Ho Y, Huang G M and Li P 2009 Nonvolatile memristor memory: device characteristics and design implications *Proceedings of the 2009 International Conference on Computer-Aided Design* pp 485–490

[31] Adamatzky A, Nikolaidou A, Gandia A, Chiolerio A and Dehshibi M M 2021 *Biosystems* **199** 104304

[32] Adamatzky A, Gandia A and Chiolerio A 2021 *Fungal biology and biotechnology* **8** 1–6

[33] Li J, Xin M, Ma Z, Shi Y and Pan L 2021 *Nanotechnology*
[34] Karana E, Blauwhoff D, Hultink E J and Camere S 2018 *International Journal of Design* **12**
[35] Jones M, Mautner A, Luenco S, Bismarck A and John S 2020 *Materials & Design* **187** 108397
[36] Cerimi K, Akkaya K C, Pohl C, Schmidt B and Neubauer P 2019 *Fungal biology and biotechnology* **6** 1–10
[37] Pelletier M, Holt G, Wanjura J, Bayer E and McIntyre G 2013 *Industrial Crops and Products* **51** 480–485
[38] Elsacker E, Vandelook S, Van Wylick A, Ruytinx J, De Laet L and Peeters E 2020 *Science of The Total Environment* **725** 138431
[39] Robertson O *et al.* 2020 *DS 101: Proceedings of NordDesign 2020, Lyngby, Denmark, 12th-14th August 2020* 1–13
[40] Yang Z, Zhang F, Still B, White M and Amstislavski P 2017 *Journal of Materials in Civil Engineering* **29** 04017030
[41] Xing Y, Brewer M, El-Gharabawy H, Griffith G and Jones P 2018 Growing and testing mycelium bricks as building insulation materials *IOP Conference Series: Earth and Environmental Science* vol 121 (IOP Publishing) p 022032
[42] Girometta C, Picco A M, Baiguera R M, Dondi D, Babbini S, Cartabia M, Pellegrini M and Savino E 2019 *Sustainability* **11** 281
[43] Dias P P, Jayasinghe L B and Waldmann D 2021 *Results in Materials* **10** 100189
[44] WANG F, LI H q, KANG S s, BAI Y f, CHENG G z and ZHANG G q 2016 *Science Technology and Engineering* **2016** 20
[45] Cárdenas-R J P 2020 Thermal insulation biomaterial based on hydrangea macrophylla *Bio-Based Materials and Biotechnologies for Eco-Efficient Construction* (Elsevier) pp 187–201
[46] Holt G, Mcintyre G, Flagg D, Bayer E, Wanjura J and Pelletier M 2012 *Journal of Biobased Materials and Bioenergy* **6** 431–439
[47] Sivaprasad S, Byju S K, Prajith C, Shaju J and Rejeesh C 2021 *Materials Today: Proceedings*
[48] Mojumdar A, Behera H T and Ray L 2021 *Microbial Polymers* 131–141
[49] Yin Z, Tian H, Chen G and Chua L O 2015 *IEEE Transactions on Circuits and Systems II: Express Briefs* **62** 402–406
[50] Schütte K H 1956 *New Phytologist* **55** 164–182
[51] Jennings D 1987 *Biological Reviews* **62** 215–243
[52] Chua L 2014 *Semiconductor Science and Technology* **29** 104001
[53] Podlubny I 1999 *Fractional Differential Equations* (Academic Press, San Diego)
[54] Chiolerio A, Draper T C, Mayne R and Adamatzky A 2020 *Journal of colloid and interface science* **560** 589–595
[55] Erokhin V and Fontana M P 2008 *arXiv preprint arXiv:0807.0333*
[56] Gale E, Pearson D, Kitson S, Adamatzky A and de Lacy Costello B 2015 *Materials Chemistry and Physics* **162** 20–30
[57] Gale E, de Lacy Costello B and Adamatzky A 2014 *Microelectronics Journal* **45** 1401–1415
[58] Serrano-Gotarredona T, Prodromakis T and Linares-Barranco B 2013 *IEEE Circuits and Systems Magazine* **13** 74–88
[59] Indiveri G, Linares-Barranco B, Legenstein R, Deligeorgis G and Prodromakis T 2013 *Nanotechnology* **24** 384010
[60] Prezioso M, Zhong Y, Gavrilov D, Merrikh-Bayat F, Hoskins B, Adam G, Likharev K and Strukov D 2016 Spiking neuromorphic networks with metal-oxide memristors *2016 IEEE International Symposium on Circuits and Systems (ISCAS)* (IEEE) pp 177–180
[61] Pickett M D, Medeiros-Ribeiro G and Williams R S 2013 *Nature materials* **12** 114–117
[62] Linares-Barranco B, Serrano-Gotarredona T, Camuñas-Mesa L A, Perez-Carrasco J A, Zamarreño-Ramos C and Masquelier T 2011 *Frontiers in neuroscience* **5** 26
[63] Indiveri G and Liu S C 2015 *Proceedings of the IEEE* **103** 1379–1397
[64] Adamatzky A, Tegelaar M, Wosten H A, Powell A L, Beasley A E and Mayne R 2020 *Biosystems*

193 104138
[65] Adamatzky A, Gandia A, Ayres P, Wösten H and Tegelaar M *LINKs-series* **5** 66–77